Fractionalization and Topology in Amorphous Electronic Solids

Sunghoon Kim,[1] Adhip Agarwala,[2,3,4] and Debanjan Chowdhury[1]

[1]*Department of Physics, Cornell University, Ithaca, New York 14853, USA*
[2]*International Center for Theoretical Sciences, Bangalore 560089, India*
[3]*Max-Planck Institute for the Physics of Complex Systems, Nöthnitzer straße 38, Dresden 01187, Germany*
[4]*Department of Physics, Indian Institute of Technology, Kanpur 208016, India*

Band topology is traditionally analyzed in terms of gauge-invariant observables associated with crystalline Bloch wave functions. Recent work has demonstrated that many of the free fermion topological characteristics survive even in an amorphous setting. In this Letter, we extend these studies to incorporate the effect of strong repulsive interactions on the fate of topology and other correlation induced phenomena. Using a parton-based mean-field approach, we obtain the interacting phase diagram for an electronic two-orbital model with tunable topology in a two-dimensional amorphous network. In addition to the (non-)topological phases that are adiabatically connected to the free fermion limit, we find a number of strongly interacting amorphous analogs of crystalline Mott insulating phases with nontrivial chiral neutral edge modes, and a fractionalized Anderson insulating phase. The amorphous networks thus provide a new playground for studying a plethora of exotic states of matter, and their glassy dynamics, due to the combined effects of nontrivial topology, disorder, and strong interactions.

Topological band theory has made a profound impact on our fundamental understanding, and in the experimental search, of weakly correlated phases of crystalline electronic solids [1–4]. A useful starting point in this endeavor is to consider crystals with perfect translational symmetry, and to include perturbative corrections due to the effects of weak disorder [5–11]. However, translational symmetry is not a prerequisite for realizing noninteracting topological phases, even in the absence of a well-defined momentum, an associated electronic "band structure," and the very notion of a Brillouin zone [12–19]. Interestingly, experiments on a candidate topological material [20] and a photonic system [21] provide promising evidence for the existence of topological phases in amorphous settings. On the theoretical front, the study of realistic models and better computational techniques continue to advance our understanding of such amorphous topological phases of free fermions [22–24].

In this Letter, we address a question of fundamental interest that has not received as much attention, except when in a crystalline setting [25–33], namely, on the effects of strong local interactions on the fate of the amorphous topological phases. The combined effects of strong interactions, topology, and disorder (manifest in the amorphous structure of the underlying network) can lead to a plethora of new phases. To study the interacting problem, we employ and adapt a parton mean-field theory [34–36] in this new amorphous setting and obtain the theoretical phase diagram for an interacting two-dimensional electronic model as a function of the strength of interactions and tunable topology. At fixed electron filling and as a function of increasing interaction strength, we find evidence of transitions into phases with deconfined fractionalized excitations, that can either support neutral edge modes (as in an amorphous Chern insulator), or display disorder-induced localization (as in an Anderson insulator) accompanied by a local inhomogeneous distribution of topological "puddles." We use a number of quantitative diagnostics for disentangling the effects of disorder and topology in order to sharpen the properties of the resulting phases and their regions of stability with increasing system sizes. While our study of a simplified theoretical model is not directly related to a realistic model of a quantum material, recent experimental work in twisted bilayer graphene [37] suggests that the notion of a "local" Chern number and a "mosaic" of distinct topological patches can emerge in the presence of long-wavelength inhomogeneities in a strongly correlated topological system. Our theoretical study highlights the incredibly rich playground provided by seemingly "disordered" systems as an exciting new platform for realizing topological and fractionalized phases of matter.

Model.—We define a two-dimensional (spinless) electronic model with local interactions, residing on an amorphous network with two orbitals (e.g., s and p) per site; see Fig. 1, inset. The Hamiltonian is of the form
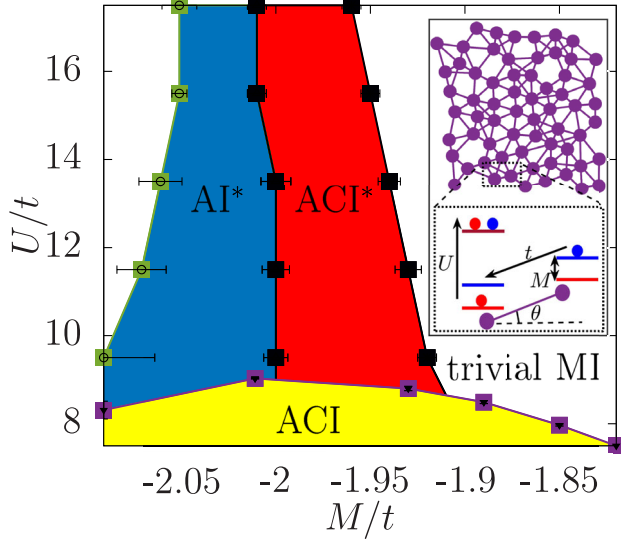
FIG. 1.   Theoretical phase diagram at half-filling as a function of M/t and U/t for system of size 16×16. The four distinct phases include a trivial electronic Mott insulator (MI), an amorphous Chern Insulator (ACI), a fractionalized Anderson insulator (AI*), and a fractionalized amorphous Chern insulator (ACI*), respectively. The inset denotes a typical amorphous network and the energy scales associated with hopping (t), orbital splitting (M). and on-site repulsion (U).

$$H = H_0 + H_{\text{int}}, \tag{1a}$$

$$H_0 = -\sum_{\substack{i \neq j \\ \alpha,\beta}} [t_{\alpha\beta}(\boldsymbol{r}_{ij})c_{i,\alpha}^\dagger c_{j,\beta} + \text{H.c.}] + \sum_{i,\alpha,\beta}\epsilon_{\alpha\beta}c_{i,\alpha}^\dagger c_{i,\beta}, \tag{1b}$$

$$H_{\text{int}} = \frac{U}{2}\sum_i \hat{N}_i(\hat{N}_i - 1), \tag{1c}$$

where $c_{i,\alpha}^\dagger(c_{i,\alpha})$ is an electron creation (annihilation) operator with orbital index α at site i and $t_{\alpha\beta}(\boldsymbol{r}_{ij})$ represents the tunneling matrix element between sites i, j separated by distance $r = |\boldsymbol{r}_{ij}|$. The on-site single-particle and interaction energies are given by $\epsilon_{\alpha\beta}$ and U, respectively, where $\hat{N}_i = \sum_\alpha c_{i,\alpha}^\dagger c_{i,\alpha}$. We assume that the tunneling matrix elements have a *statistical* rotational symmetry with an exponential fall-off with distance over a characteristic scale, a_B, and vanish beyond $r = R$, i.e., $t_{\alpha\beta}(\boldsymbol{r}) = t(r)T_{\alpha\beta}(\hat{\boldsymbol{r}})$ where $t(r) = C\Theta(R - r)\exp(-r/a_B)$ and C is a constant chosen such that $t(r = a_B) = 1$. All other energy scales are scaled with respect to this unit scale. The orbital dependence of the single-particle energy and tunneling matrix element is given by

$$\epsilon_{\alpha\beta} = \begin{pmatrix} 2t + M & 0 \\ 0 & -(2t + M) \end{pmatrix}, \tag{2a}$$

$$T_{\alpha\beta}(\hat{\boldsymbol{r}}) = \frac{1}{2}\begin{pmatrix} -1 & -ie^{-i\theta} \\ -ie^{i\theta} & 1 \end{pmatrix}, \tag{2b}$$

where θ is the angle subtended between a reference axis and the vector $\hat{\boldsymbol{r}}$ connecting sites i and j (see inset of Fig. 1), and M modulates the on-site energy of the orbitals. The sites that make up the amorphous graph are constructed randomly, but with a minimal exclusion distance, $r_{\min}$.

In the noninteracting limit ($U = 0$), H belongs to class A of the tenfold classification with broken time-reversal symmetry, and where previous Letter has pointed out the existence of free fermion topological phases with robust edge states as a function of varying M, a_B [12]. These phases exist over a large window of a_B, $r_{\min}$ [38], and it is straightforward to generalize these results to other classes of the tenfold way. In the remainder of this Letter, we obtain the phase diagram of H as a function of U/t, M/t, where the complex interplay of interactions, topology and the amorphous nature of the underlying graph reveals interesting phases of matter (Fig. 1). In the remainder of our study, we set $a_B = 1$, $R = 1.5$, and $r_{\min} = 0.8$, unless stated otherwise.

To analyze the fate of the Hamiltonian at large U, we use the parton construction for the electronic operators, $c_{i,\alpha} = b_i f_{i,\alpha}$, in terms of a bosonic, electrically charged "rotor" field ($b_i = e^{i\theta_i}$) and a neutral fermion ($f_{i,\alpha}$) [34,35]. However, given the amorphous nontranslationally invariant connectivity, we employ a new implementation of the two-site cluster mean field theory to obtain the phase diagram. The method does not necessarily capture details of the energetics associated with the true many-body ground state, but provides a self-consistent solution within the parton mean-field approximation. We will refer to the fermionic excitations, $f_{i,\alpha}$, as "spinons" even though they are not tied to any underlying fractionalization associated with an actual spin degree of freedom.

In terms of the new fields, the Hamiltonian is given by

$$H_0 = -\sum_{\substack{i \neq j \\ \alpha\beta}} [t_{\alpha\beta}(\boldsymbol{r}_{ij})f_{i,\alpha}^\dagger b_i^\dagger b_j f_{j,\beta} + \text{H.c.}] + \sum_{i,\alpha,\beta}\epsilon_{\alpha\beta}f_{i,\alpha}^\dagger f_{i,\beta},$$

$$H_{\text{int}} = \frac{U}{2}\sum_i (\hat{L}_i - 1)(\hat{L}_i - 2) \tag{3}$$

where we have used the physical Hilbert space constraint $L_i + \sum_\alpha n_{i,\alpha}^f = 2$ with $\hat{L}_i = (\partial/\partial\theta_i)$ and $\langle N_i \rangle = \sum_\alpha \langle n_{i,\alpha}^f \rangle$. We include a chemical potential to maintain half-filling of electrons which imposes $\langle \sum_\alpha n_{i,\alpha}^f \rangle = 1$ and $\langle L_i \rangle = 1$ at every site i for both spinons and rotors. We carry out a mean-field decoupling of $H_0 \to H_b + H_f$, where nominally H_f is described by a free Hamiltonian [38]. However, the fermion hoppings are renormalized by the rotor correlators, $\langle b_i^\dagger b_j \rangle$. As noted earlier, to solve for the
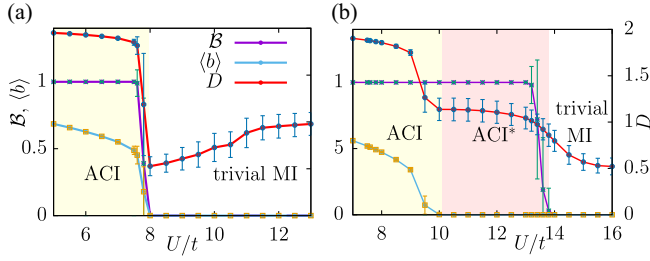
FIG. 2. Bott index ($\mathcal{B}$), superfluid order parameter $\langle b \rangle$, and the rotor fractal dimension D in system of size 16×16 for a fixed (a) $M/t = -1.84$, and (b) $M/t = -1.94$, respectively, obtained by averaging over 100 uncorrelated amorphous configurations.

interacting rotor Hamiltonian, $H_b + H_{int}$, we use a two-site cluster mean field theory for *every* pair of connected sites on the amorphous graph. We calculate the superfluid order parameter on every site $\langle b_i \rangle$, and the fermionic correlators between pairs of sites $\langle f^{\dagger}_{i,\alpha} f_{j,\beta} \rangle$ self-consistently until the results converge.

Fractionalized phases.—Our solution suggests that for $U \lesssim 9t$, the rotors are condensed in a superfluid phase with $\langle b \rangle = \sum_i \langle b_i \rangle / N [\sim O(1)]$, which is consistent with the typical values even in nontopological and crystalline systems [34,35]. As a function of M/t, the spinon "bands" realize both topological and trivial phases, respectively (Fig. 1). A nonzero $\langle b \rangle \neq 0$ corresponds to a confined phase with a renormalized electronic quasiparticle residue; the two phases described above correspond to a trivial electronic insulator and an amorphous electronic Chern insulator which are adiabatically connected to the $U = 0$ limit [12].

To diagnose the topological properties for the spinons in the absence of translational invariance and a notion of a Brillouin zone, we evaluate their *Bott index* ($\mathcal{B}$) which quantifies the noncommutativity of the position operators when projected to the lower band of the spinon system [12,39]. The index is given by

$$\mathcal{B} = \frac{1}{2\pi} \text{Im}\{\text{tr}[\log(WUW^{\dagger}U^{\dagger})]\} \qquad (4)$$

where $U = P \exp(i\Theta)P$, $W = P \exp(i\Phi)P$, and $P = \sum_m |m\rangle\langle m|$ is the projector made of all occupied spinonic wave functions $|m\rangle$. Θ, Φ are diagonal matrices whose elements correspond to the real space positions of every orbital $(x_{i\alpha}, y_{i\alpha})$, but compactified into a torus $(2\pi x_{i\alpha}/L, 2\pi y_{i\alpha}/L)$, where L is the linear dimension of the system. $\mathcal{B}$ is thus a generalization of the usual Chern number, but in a setting where translational symmetry is completely absent.

At larger values of U/t, we find two new correlation-induced phases [Figs. 2(a) and 2(b)]. Depending on the value of M/t, we find distinct insulating regimes. For example, for $M/t \sim -1.84$ and as a function of increasing

U/t, the superfluid order $\langle b \rangle$ goes to zero across $U = U_c$. Across the same transition, and within our numerical resolution, the Bott index jumps from 1 to 0. Interestingly, both of these changes across $U \sim U_c$ occur over any typical configuration, such that configuration averaged quantities [$\sim O(100)$ configurations] also reflect a relatively sharp transition. The latter phase is clearly a topologically trivial Mott insulator realized at half-filling due to strong correlation effect. Even while $\langle b \rangle$ goes to zero, there are rare regions in the system where the superfluid (SF) order parameter is vanishingly small, yet finite, which results in intrinsic inhomogeneities in this system, which we discuss in detail later in the Letter. In contrast, for $M/t \sim -1.94$, there is an intermediate phase over $U_{c1} < U < U_{c2}$ where the rotors are Mott insulating with $\langle b \rangle = 0$, while the Bott index remains pinned at 1. This intermediate phase is a novel example of an electronic Mott insulator where the spinons inherit nontrivial topology in an amorphous setting. As we discuss below, when defined in an open system with boundaries, the phase is defined by protected electrically *neutral* chiral edge modes that can carry a finite energy. We dub this phase as the fractionalized *amorphous* Chern insulator (ACI*). We note that the fractionalized phases appear near $M/t \sim -2$, which corresponds to the critical point of the noninteracting crystalline model. This can be understood by noting that the intersite fermionic hopping gets renormalized by the rotor correlators at large U/t, which then effectively reduces the spinonic bandwidth around $M/t = -2$. The nontrivial features of the spinonic band are likely to manifest near a window of $M/t \sim -2$. While the phase occurs over a small window of parameter space, our calculations with increasing system size suggest that they survive even in the thermodynamic limit [38].

Glassy physics.—A key element in our study is the inherently disordered nature of the amorphous network, which can lead to "glassy" physics and strong local inhomogeneities. At small U/t, we find that the disorder induced "rare-region" effects are relatively suppressed in the rotor superfluid and associated electronic trivial or Chern insulators; the distribution of site-resolved local superfluid order does not develop strong inhomogeneity. However, with increasing U/t, the amorphous network develops strong local inhomogeneities in the vicinity of the Mott transition. To characterize this phenomenology, we compute the fractal dimension for the rotors as [40],

$$D = \log_L \left(\frac{\sum_{i=1}^N |\langle b_i \rangle|^2}{\max_i |\langle b_i \rangle|^2} \right), \qquad (5)$$

where i is the position index, L is the linear dimension, and N is the total number of sites. D is useful for characterizing the effective dimensionality of the largest SF patch in the system. We note that when the rotors are condensed and the superfluid order is relatively homogeneous across the
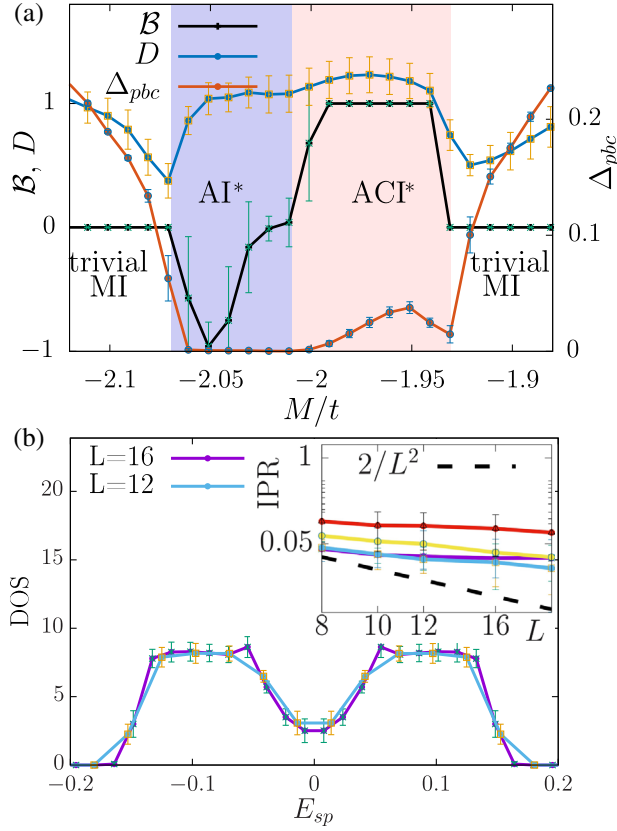
FIG. 3. (a) Configuration averaged quantities (D, $\mathcal{B}$, and Δ_{pbc}) for a 16×16 system at $U/t = 12$ with periodic boundary conditions. (b) The spinon DOS in the AI* phase at $M/t = -2.05$, normalized by the total energy integrated DOS. Inset: the spinon IPR at the Fermi level for five different representative M/t values in the AI* phase [-2.05 (violet) $\leq M/t \leq -2.02$ (red)] for increasing system size. The black dashed line marks the IPR of a homogeneous system.

system, D approaches a value ~ 2. On the other hand, across the Mott transition and regardless of whether the resulting insulator is (non-)topological, we find that D develops a characteristic kink showing the rotor SF-to-Mott insulator (MI) transition happens in a nonuniform way over the network. In contrast, for a crystalline system, a MI state when diagnosed on finite size lattices have an infinitesimally small but *uniform* SF order parameter which implies D remains ~ 2 [38]. Here, the characteristic kink in D reflects the realization of a Bose-glass phase. That the transition is thermodynamically stable is reflected in the systematic system size scaling [38], where the kink remains even as system size is increased. Our discussion so far has focussed on the effects of inhomogeneities in the boson sector. Next we shift our attention to the fermions.

In the ACI* phase, the f fermions have a finite gap, Δ_{pbc}, at half-filling [with $\langle b \rangle = 0$]. Near $M/t \sim -2$, the spinon hopping competes with disorder energy scales mixing the two orbitals, leading to three distinct regimes [Fig. 3(a)]: (i) for $M \lesssim -2.1t$ and $M \gtrsim -1.9t$, $\Delta_{pbc} \neq 0$, and $\mathcal{B} = 0$,

(ii) for $-2t \lesssim M \lesssim -1.9t$, $\Delta_{pbc} \neq 0$ but $\mathcal{B} = 1$, and (iii) for $-2.1t \lesssim M \lesssim -2t$, $\Delta_{pbc} \to 0$ while $\mathcal{B} \sim -1$ (see below). Over the entire range of M/t values and large U/t considered above, $\langle b \rangle \to 0$ and $D < 2$, which signifies that all of the phases are electrical insulators affected strongly by the inhomogeneity in the amorphous network. We have already discussed the origin of the interesting behavior in regions (i) and (ii) above. We note that these transitions are expected to remain sharp in the thermodynamic limit, as shown by the system size scaling [38].

In region (iii), the "gapless" phase ($\Delta_{pbc} \to 0$) is not tied to any itinerant fermions, but arises instead due to localization on the amorphous network, as can be seen by calculating the inverse participation ratio (IPR),

$$\mathrm{IPR}_m = \frac{1}{2L^2} \sum_{i,\alpha} |\psi_{m,i\alpha}|^4, \tag{6}$$

and the density of states (DOS) near the Fermi-energy. Here, $\psi_{m,i\alpha} = \langle i\alpha | m \rangle$ denotes the spinon wave function ($|m\rangle$) associated with orbital α on the ith site, and has been calculated from an explicit diagonalization of the mean-field Hamiltonian, H_f. We find a finite DOS at the Fermi level in the absence of a gap [see Fig. 3(b)]; additionally, the IPR from the fermionic states is much larger than a typical delocalized state ($\sim 1/2L^2$) [inset of Fig. 3(b)]. All of these observables are then consistent with a disorder induced localization of neutral spinons, and hence we dub it as a fractionalized Anderson insulator (AI*). Interestingly, the seemingly nontrivial topological character associated with the large fluctuations of $\mathcal{B}$ near -1 is due to local topological "puddles," associated with different disorder realizations.

Finally, to help clarify the topological character associated with the fractionalized phases, we also calculate a "local Chern marker" for a representative configuration in both the AI* and ACI* phases, respectively. The local Chern marker is defined as [41],

$$C(\mathbf{r}) = -2\pi i \mathrm{Tr}\{[PxP, PyP]\}, \tag{7}$$

where P is the projector, as defined earlier. The results for $C(\mathbf{r})$ for typical networks of size 24×24 are shown in Figs. 4(a) and 4(b). In the ACI* phase, $C(\mathbf{r})$ is approximately uniformly distributed in the bulk [Fig. 4(a)], while it exhibits stronger fluctuations in the AI* phase [Fig. 4(b)] [38]. These observations are reflected in the location of the edge states in open systems. While the ACI* has spinon edge states [Fig. 4(c)], the distinction between bulk and edge states is unclear in the AI* phase [Fig. 4(d)]. Thus even though $\mathcal{B}$ fluctuates strongly near -1 in the particular realization of the AI* phase in Fig. 4(b), there is no clear sign of an edge state, and the midgap states are localized sporadically throughout the system. In particular, often wave functions are localized inside the bulk but
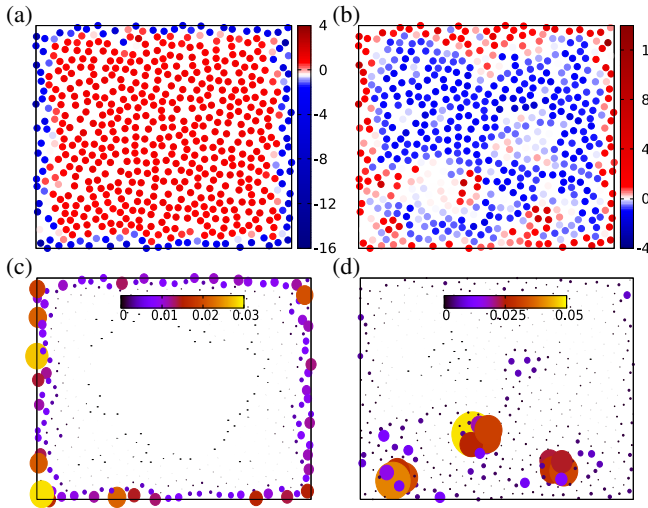
FIG. 4. The local Chern marker (top) and the midgap state distribution (bottom) of the ACI* phase (left (a) and (c)) and the AI* phase (right (b) and (d)) with open boundary conditions $(24 \times 24$ system). For the midgap state distribution, the size and the color of a blob quantify the probability of finding a spinon at that site. In the ACI* phase, (a) and (c) show clear signs of a gapless edge state.

between two domains of differently oriented local Chern marker patches reflecting development of edgelike states but on effective grain boundaries. How such patches determine the physical characteristics of a thermodynamic phase and its properties is an interesting direction for future work.

It is interesting to note that the disordered AI* phase only occurs in the $\mathcal{B} = -1$ regime. This has to do with the underlying noninteracting dispersion in the crystalline case, where the topological transitions are accompanied by Dirac cone closings at the Γ point, $(0, \pi)$, $(\pi, 0)$, and (π, π), respectively. The transition to the $C = 1$ phase arises at the Γ point, which is more resilient in the amorphous setting. On the other hand, the transitions to the $C = -1$ phase arises at the large momentum points, which are more susceptible to the inhomogeneity associated with the amorphous network.

Outlook.—In this Letter, we have analyzed the effects of strong correlations in the presence of nontrivial topology in an amorphous setting at the level of parton mean-field theory. None of the excitations we have obtained in the insulating bulk of these phases are itinerant. By including additional local degrees of freedom and by extending the analysis to higher dimensions [42], it will be interesting to analyze the possibility of hosting a diffusive spinon metal in a bulk electrical insulator coexisting with topological surface states. Going beyond the parton mean-field analysis, it is natural to address the effects of emergent gauge-field fluctuations, which are a defining feature of the fractionalized phases [43–46]. In our simplified construction of the ACI* phase, the total Bott index for the spinons

is $\mathcal{B} = 1$; in the analogous crystalline setup with Chern number 1, the topological order and edge states can be gauged away [47]. While we leave a detailed analysis of such effects for future work, a clear direction to explore further is to construct amorphous models with higher $\mathcal{B}$, where the edge states cannot simply be gauged away. Similarly, in the AI* phase, the subtle interplay between disorder-induced localization and a tendency towards confinement in the presence of topological puddles is an interesting direction for future work. Finally, the platform considered here is ideally suited for studying the effects of nontrivial topology and fractionalization on their non-equilibrium glassy dynamics.

[1] A. W. W. Ludwig, Topological phases: Classification of topological insulators and superconductors of non-interacting fermions, and beyond, Phys. Scr. **T168**, 014001 (2016).

[2] C.-K. Chiu, J. C. Y. Teo, A. P. Schnyder, and S. Ryu, Classification of topological quantum matter with symmetries, Rev. Mod. Phys. **88**, 035005 (2016).

[3] M. Z. Hasan and C. L. Kane, Colloquium: Topological insulators, Rev. Mod. Phys. **82**, 3045 (2010).

[4] X.-L. Qi and S.-C. Zhang, Topological insulators and superconductors, Rev. Mod. Phys. **83**, 1057 (2011).

[5] D. N. Sheng, Z. Y. Weng, L. Sheng, and F. D. M. Haldane, Quantum Spin-Hall Effect and Topologically Invariant Chern Numbers, Phys. Rev. Lett. **97**, 036808 (2006).

[6] C. Xu and J. E. Moore, Stability of the quantum spin hall effect: Effects of interactions, disorder, and F_2 topology, Phys. Rev. B **73**, 045322 (2006).

[7] C. Wu, B. A. Bernevig, and S.-C. Zhang, Helical Liquid and the Edge of Quantum Spin Hall Systems, Phys. Rev. Lett. **96**, 106401 (2006).

[8] M. Onoda, Y. Avishai, and N. Nagaosa, Localization in a Quantum Spin Hall System, Phys. Rev. Lett. **98**, 076802 (2007).

[9] Q. Liu, C.-X. Liu, C. Xu, X.-L. Qi, and S.-C. Zhang, Magnetic Impurities on the Surface of a Topological Insulator, Phys. Rev. Lett. **102**, 156603 (2009).

[10] A. Medhi, V. B. Shenoy, and H. R. Krishnamurthy, Synchronous and asynchronous mott transitions in topological insulator ribbons, Phys. Rev. B **85**, 235449 (2012).

[11] I. C. Fulga, F. Hassler, and A. R. Akhmerov, Scattering theory of topological insulators and superconductors, Phys. Rev. B **85**, 165409 (2012).

[12] A. Agarwala and V. B. Shenoy, Topological Insulators in Amorphous Systems, Phys. Rev. Lett. **118**, 236402 (2017).

[13] N. P. Mitchell, L. M. Nash, D. Hexner, A. M. Turner, and W. T. Irvine, Amorphous topological insulators constructed from random point sets, Nat. Phys. **14**, 380.

[14] K. Pöyhönen, I. Sahlberg, A. Weström, and T. Ojanen, Amorphous topological superconductivity in a shiba glass, Nat. Commun. **9**, 2103 (2018).

[15] G.-W. Chern, Topological insulator in an atomic liquid, Europhys. Lett. **126**, 37002 (2019).

[16] M. Costa, G. R. Schleder, M. Buongiorno Nardelli, C. Lewenkopf, and A. Fazzio, Toward realistic amorphous topological insulators, Nano Lett. **19**, 8941 (2019).

[17] Y.-B. Yang, T. Qin, D.-L. Deng, L.-M. Duan, and Y. Xu, Topological Amorphous Metals, Phys. Rev. Lett. **123**, 076401 (2019).

[18] H. Spring, A. Akhmerov, and D. Varjas, Amorphous topological phases protected by continuous rotation symmetry, SciPost Phys. **11**, 022 (2021).

[19] A. Agarwala, V. Juricic, and B. Roy, Higher-order topological insulators in amorphous solids, Phys. Rev. Res. **2**, 012067(R) (2020).

[20] P. Corbae, S. Ciocys, D. Varjas, E. Kennedy, S. Zeltmann, M. Molina-Ruiz, S. Griffin, C. Jozwiak, Z. Chen, L.-W. Wang, A. M. Minor, M. Scott, A. G. Grushin, A. Lanzara, and F. Hellman, Evidence for topological surface states in amorphous Bi_2Se_3, arXiv:1910.13412.

[21] P. Zhou, G.-G. Liu, X. Ren, Y. Yang, H. Xue, L. Bi, L. Deng, Y. Chong, and B. Zhang, Photonic amorphous topological insulator, Light **9**, 133 (2020).

[22] Q. Marsal, D. Varjas, and A. G. Grushin, Topological weaire–thorpe models of amorphous matter, Proc. Natl. Acad. Sci. U.S.A. **117**, 30260 (2020).

[23] M. N. Ivaki, I. Sahlberg, and T. Ojanen, Criticality in amorphous topological matter: Beyond the universal scaling paradigm, Phys. Rev. Res. **2**, 043301 (2020).

[24] B. Focassio, G. R. Schleder, F. Crasto de Lima, C. Lewenkopf, and A. Fazzio, Amorphous bi_2se_3 structural, electronic, and topological nature from first principles, Phys. Rev. B **104**, 214206 (2021).

[25] J. Maciejko, X.-L. Qi, A. Karch, and S.-C. Zhang, Fractional Topological Insulators in Three Dimensions, Phys. Rev. Lett. **105**, 246809 (2010).

[26] S. Rachel and K. Le Hur, Topological insulators and mott physics from the hubbard interaction, Phys. Rev. B **82**, 075106 (2010).

[27] D. Pesin and L. Balents, Mott physics and band topology in materials with strong spin–orbit interaction, Nat. Phys. **6**, 376 (2010).

[28] J. He, S.-P. Kou, Y. Liang, and S. Feng, Chiral spin liquid in a correlated topological insulator, Phys. Rev. B **83**, 205116 (2011).

[29] B. Swingle, M. Barkeshli, J. McGreevy, and T. Senthil, Correlated topological insulators and the fractional magnetoelectric effect, Phys. Rev. B **83**, 195139 (2011).

[30] J. Maciejko and G. A. Fiete, Fractionalized topological insulators, Nat. Phys. **11**, 385 (2015).

[31] S. Rachel, Interacting topological insulators: A review, Rep. Prog. Phys. **81**, 116501 (2018).

[32] C. Hickey, P. Rath, and A. Paramekanti, Competing chiral orders in the topological haldane-hubbard model of spin-$\frac{1}{2}$ fermions and bosons, Phys. Rev. B **91**, 134414 (2015).

[33] B. Roy, P. Goswami, and J. D. Sau, Continuous and discontinuous topological quantum phase transitions, Phys. Rev. B **94**, 041101(R) (2016).

[34] S. Florens and A. Georges, Slave-rotor mean-field theories of strongly correlated systems and the mott transition in finite dimensions, Phys. Rev. B **70**, 035114 (2004).

[35] E. Zhao and A. Paramekanti, Self-consistent slave rotor mean-field theory for strongly correlated systems, Phys. Rev. B **76**, 195101 (2007).

[36] A. C. Potter, M. Barkeshli, J. McGreevy, and T. Senthil, Quantum Spin Liquids and the Metal-Insulator Transition in Doped Semiconductors, Phys. Rev. Lett. **109**, 077205 (2012).

[37] S. Grover, M. Bocarsly, A. Uri, P. Stepanov, G. Di Battista, I. Roy, J. Xiao, A. Y. Meltzer, Y. Myasoedov, K. Pareek, K. Watanabe, T. Taniguchi, B. Yan, A. Stern, E. Berg, D. K. Efetov, and E. Zeldov, Imaging Chern mosaic and Berry-curvature magnetism in magic-angle graphene, Nat. Phys. **18**, 885 (2022).

[38] See Supplemental Material at http://link.aps.org/supplemental/10.1103/PhysRevLett.130.026202 for additional details on the mean-field decompositions, noninteracting limit, scaling of observables as a function of system size, a distribution of the Chern markers in the ACI* and AI* phases, and comparisons with the crystalline limit.

[39] M. B. Hastings and T. A. Loring, Topological insulators and c-algebras: Theory and numerical practice, Ann. Phys. (Amsterdam) **326**, 1699 (2011).

[40] A. Geißler, Finite-size scaling analysis of localization transitions in the disordered two-dimensional bose-hubbard model within the fluctuation operator expansion method, Phys. Rev. A **103**, 043332 (2021).

[41] R. Bianco and R. Resta, Mapping topological order in coordinate space, Phys. Rev. B **84**, 241106(R) (2011).

[42] P. Mukati, A. Agarwala, and S. Bhattacharjee, Topological and conventional phases of a three-dimensional electronic glass, Phys. Rev. B **101**, 035142 (2020).

[43] L. B. Ioffe and A. I. Larkin, Gapless fermions and gauge fields in dielectrics, Phys. Rev. B **39**, 8988 (1989).

[44] P. A. Lee, N. Nagaosa, and X.-G. Wen, Doping a mott insulator: Physics of high-temperature superconductivity, Rev. Mod. Phys. **78**, 17 (2006).

[45] D. Chowdhury, I. Sodemann, and T. Senthil, Mixed-valence insulators with neutral fermi surfaces, Nat. Commun. **9**, 1766 (2018).

[46] T. Senthil, Theory of a continuous mott transition in two dimensions, Phys. Rev. B **78**, 045109 (2008).

[47] X.-G. Wen, *Quantum Field Theory of Many-Body Systems: From the Origin of Sound to an Origin of Light and Electrons* (Oxford University Press, Oxford, 2004).